Electric Polarization, Magnetoelectric Effect, and Orbital State of a Layered Iron Oxide with Frustrated Geometry

A. Nagano,* M. Naka, J. Nasu, and S. Ishihara

Department of Physics, Tohoku University, Sendai 980-8578, Japan

(Received 4 February 2007; published 19 November 2007)

A layered iron oxide $R\mathrm{Fe_2O_4}$ (R denotes rare-earth-metal elements) is an exotic dielectric material with charge-order (CO) driven electric polarization and magnetoelectric effect caused by spin-charge coupling. In this paper, a theory of electronic structure and dielectric property in $R\mathrm{Fe_2O_4}$ is presented. Charge frustration in paired-triangular lattices allows a charge imbalance without inversion symmetry. Spin frustration induces reinforcement of this polar CO by a magnetic ordering. We also analyze an orbital model for the Fe ion which does not show a conventional long-range order.

DOI: 10.1103/PhysRevLett.99.217202 PACS numbers: 75.80.+q, 72.80.Ga, 75.10.−b, 77.80.−e

Ferroelectric (FE) material has a spontaneous electric polarization induced by displacement of ion and electronic cloud. A subtle balance of long-range Coulomb interaction, lattice potential, and electron covalency derives the FE transition and controls the transition temperature. Recently revived magnetoelectric (ME) effects and related multiferroic phenomena [1–3] are recognized as spin-driven FE transitions. A key issue is a noncollinear spin structure in frustrated magnets where lattice displacement without inversion symmetry is induced by the symmetric and/or antisymmetric exchange strictions. Because of the observed gigantic ME effects, this type of materials has been examined from the viewpoint of potential application as well as fundamental physics.

When electronic charges are ordered without inversion symmetry, a macroscopic electric polarization appears in a crystal. This can be another mechanism for ferroelectricity. This new class of ferroelectricity, which we call "electronic" ferroelectricity, is examined recently in the charge ordered manganites [4,5] and several organic salts [6,7]. Rare-earth-metal iron oxides $R\mathrm{Fe_2O_4}$ (R denotes rare-earth-metal elements) [8] of the present interest belong to this class of materials. The crystal structure consists of paired Fe-O triangular lattices [Fig. 1(a)] and R-O block ones alternately stacked along the c axis. Since a nominal valence of Fe ion is 2.5 + , an equal amount of $\mathrm{Fe^{2+}}$ and $\mathrm{Fe^{3+}}$ coexists in the paired-triangular lattices. In the electron diffraction experiments, Bragg reflections at $(\frac{h}{3}\ \frac{h}{3}\ 3m + \frac{1}{2})$ appear below 320 K($\equiv T_{\mathrm{CO}}$) in $\mathrm{LuFe_2O_4}$. This observation indicates a charge order (CO) of the Fe $3d$ electrons [9]. Around T_{CO}, an electric polarization and dielectric anomalies turn up [10]. Moreover, around the ferrimagnetic spin ordering (SO) temperature ($T_{\mathrm{SO}} =$ 250 K) [11,12], the ME effects are recently discovered [10,13,14].

These experiments imply that $R\mathrm{Fe_2O_4}$ is not only a CO driven FE, but also a multiferroic material due to charge-spin coupling. A possibility of such multiferroic materials ubiquitously exist in transition-metal oxides and organic salts. In this Letter, we present a theory of a dielectric magnet $R\mathrm{Fe_2O_4}$ as an electronic ferroelectric and multiferroic material. We address the following issues: (i) origin of the electric polarization, (ii) mechanism of the coupling between electric polarization and magnetization, and (iii) orbital structure of the Fe ion. The present study shows that the novel dielectric properties in $R\mathrm{Fe_2O_4}$ arise from interplay among the geometrical frustration and the multi degrees of freedom of electron.

Start with the electronic structure in a single Fe ion in $R\mathrm{Fe_2O_4}$. An Fe ion is fivefold coordinate with three O anions in the plane and two at apices [8]. We calculate the crystalline-field splitting for the $3d$ orbitals in a $\mathrm{FeO_5}$ cluster based on the point-charge model. Split orbitals are assigned to the irreducible representation for the D_{3d} group: the $d_{3z^2-r^2}$ (A') orbital, and two sets of the doubly degenerate orbitals, $\{ad_{yz} - bd_{xy}, ad_{zx} + bd_{x^2-y^2}\}$ (E'') and $\{ad_{xy} + bd_{yz}, ad_{x^2-y^2} - bd_{zx}\}$ (E'), where $a^2 + b^2 = 1$. The degenerate E' orbitals take the lowest energy with $a = 0.89$, although the energy levels for E' and E'' are close. Thus, each d orbital is singly occupied in $\mathrm{Fe^{3+}}$ ($S = 5/2$), and one of the lowest degenerate orbitals is doubly occupied in $\mathrm{Fe^{2+}}$ ($S = 2$), which has the orbital degree of freedom [15]. This is treated by the pseudospin (PS) operator with amplitude of 1/2: $\mathbf{T}_i = \frac{1}{2}\sum_{\xi,\xi',s} d^{\dagger}_{i\xi s}\sigma_{\xi\xi'}d_{i\xi' s}$ where $d_{i\xi s}$ is the electron annihilation operator with spin s and orbital ξ at site i, and σ are the Pauli matrices.

Now we set up the model Hamiltonian to describe the electronic structures and dielectric properties. The electrical resistivity in $R\mathrm{Fe_2O_4}$ shows an insulating behavior even

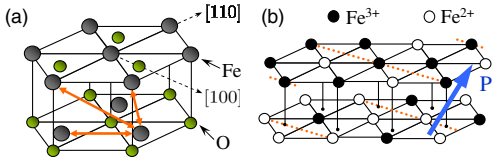

FIG. 1 (color online). (a) A pair of the Fe-O triangular lattices. Thick arrows represent the Coulomb interactions V_{abNN}, V_{cNN} and V_{cNNN}. (b) A schematic view of $\mathrm{CO}_{1/3}$ accompanied by the electric polarization.

above T_{CO} [8]. This result implies that the $3d$ electrons are almost localized at Fe ions, and incoherent charge motion occurs by thermal hopping between Fe^{2+} and Fe^{3+}. In such insulating systems, the long-range Coulomb repulsion and the superexchange interaction play major roles on dielectric and magnetic properties. The Coulomb interaction Hamiltonian $\mathcal{H}_V = \sum_{(ij)} V_{ij} n_i n_j$ with the electron number n_i is mapped onto the Ising Hamiltonian $\mathcal{H}_V = \sum_{(ij)} V_{ij} Q_i^z Q_j^z$. Here, we introduce the PS operator Q_i^z for charge which takes $1/2$ ($-1/2$) for Fe^{3+} (Fe^{2+}). The superexchange interaction arises from the virtual electron hopping between Fe ions. The Hamiltonian is derived from the generalized pd model where the on-site Coulomb and exchange interactions for the Fe $3d$ and O $2p$ electrons and the electron hopping t_{pd} between the in-plane NN sites are introduced. Since the Coulomb interactions are larger than t_{pd}, the projection-perturbation theory up to $O(t_{pd}^4)$ is applied [16]. The high-spin states at Fe ions are chosen as initial states, and all possible intermediate states are taken into account. The obtained Hamiltonian is classified by the valences of the NN Fe ions as $\mathcal{H}_J = \mathcal{H}_{22} + \mathcal{H}_{33} + \mathcal{H}_{23}$, where $\mathcal{H}_{nm}$ is for the interaction between Fe^{n+} and Fe^{m+}. Each term includes the several exchange processes denoted by Γ as $\mathcal{H}_{nm} = \sum_\Gamma \mathcal{H}_{nm}^{(\Gamma)}$. We explicitly show one dominant term in $\mathcal{H}_{22}$,

$$\mathcal{H}_{22}^{(1)} = J_{22}^{(1)} \frac{1}{5} \sum_{\langle ij \rangle} \left(\frac{1}{2}\mathbf{I}_i \cdot \mathbf{I}_j + 3\right)\left(\frac{1}{2} - 2\pi_i^{l_i}\pi_j^{l_j}\right) \times \left(\frac{1}{2} - Q_i^z\right)\left(\frac{1}{2} - Q_j^z\right). \quad (1)$$

Here, $\mathbf{I}_i$ is the spin operator with an amplitude of 2, and $J_{22}^{(1)}$ is the exchange constant. We introduce the orbital PS operators π_i^l for the three kinds of the in-plane nearest-neighbor (NN) Fe-O bond directions, labeled by $l = (a, b, c)$. These are defined by $\pi_i^l = \cos(2\pi n_l/3) T_i^z + \sin(2\pi n_l/3) T_i^x$ with $(n_a, n_b, n_c) = (0, 1, 2)$. Details in $\mathcal{H}_J$ will be presented elsewhere. It is clearly shown that spin $\mathbf{I}_i$, charge Q_i^z and orbital π_i^l are coupled with each other. Among the several interactions, the intersite Coulomb repulsion takes the largest energy scale. Thus, with lowering temperature (T), the charge sector will be frozen, at first. The expected spin ordering temperature is larger than that for the orbital because of the large magnitude of the spin operator, 2 and $5/2$.

First we focus on the origin of the CO transition accompanied by the electric polarization. We pay attention to the polar CO state characterized by the momentum $\mathbf{q} = (1/3, 1/3, 0) \equiv \mathbf{q}_3$ [see in Fig. 1(b)]. As suggested by Yamada and co-workers [9], this CO, which we call $CO_{1/3}$, shows the electric polarization due to the charge imbalance between the triangular lattices. Along [110], charge alignments are schematically ●○●●○● in the upper layer, and ●○○●○○ in the lower one, where ○ (●) represents Fe^{2+} (Fe^{3+}). This $CO_{1/3}$ competes with the nonpolar CO with $\mathbf{q} = (1/2, 0, 0) \equiv \mathbf{q}_2$ ($CO_{1/2}$), and that with $(1/4, 1/4, 1/2) \equiv \mathbf{q}_4$ ($CO_{1/4}$) [see insets of Fig. 2(c)]. In both of $CO_{1/2}$ and $CO_{1/4}$, equal numbers of Fe^{2+} and Fe^{3+} exist in the lower and upper layers, and the electric polarization does not turn up.

To examine stability of the polar $CO_{1/3}$, we analyze $\mathcal{H}_V$ in a pair of the triangular lattices, which is the minimal unit for the electric polarization. We introduce the largest three interactions V_{ij} [see Fig. 1(a)]: the interlayer NN interaction (V_{cNN}), the intralayer NN one (V_{abNN}) and the interlayer next-nearest-neighbor (NNN) one (V_{cNNN}). When the $1/r$-type Coulomb interaction is assumed, we have $V_{cNN}/V_{abNN} = 1.2$ and $V_{cNNN}/V_{abNN} = 0.77$ for $LuFe_2O_4$. In the case of $V_{cNN} = V_{cNNN} = 0$, the above three CO's are the degenerate ground states (GS). Before going to precise calculations, we have performed the mean-field (MF) calculation to obtain a global phase diagram. At $T = 0$, $CO_{1/2}$ ($CO_{1/4}$) appears in the region of $2V_{cNNN} > V_{cNN}$ ($2V_{cNNN} < V_{cNN}$), and only on the phase boundary, $CO_{1/3}$ appears. At finite T [Fig. 2(a)], we have found that $CO_{1/3}$ is stabilized in a wide region between $CO_{1/2}$ and $CO_{1/4}$.

Unbiased calculations have been performed by utilizing the Monte Carlo (MC) simulation. A pair of the triangular lattices of $L \times L$ sites ($L = 6, 12$) with periodic-boundary condition is analyzed by the multicanonical MC (MUMC) methods [17], where 8×10^6 MC steps are used for measurement. The resulting charge-correlation functions $N(\mathbf{q}) = L^{-2} \sum_{ij} \langle Q_i^z Q_j^z \rangle e^{i\mathbf{q}\cdot(\mathbf{r}_i - \mathbf{r}_j)}$ [Figs. 2(b) and 2(c)] are qualitatively consistent with the MF phase diagram. At $V_{cNNN}/V_{abNN} = 0.6$ [Fig. 2(b)], $N(\mathbf{q}_3)$ shows a hump around $T/V_{abNN} = 0.18$ and keeps the largest value down to low T. On the other hand, at $V_{cNNN}/V_{abNN} = 0.5(0.7)$ [Fig. 2(c)], a dominant charge-correlation function changes from $N(\mathbf{q}_3)$ to $N(\mathbf{q}_2)$ [$N(\mathbf{q}_4)$] with decreasing T.

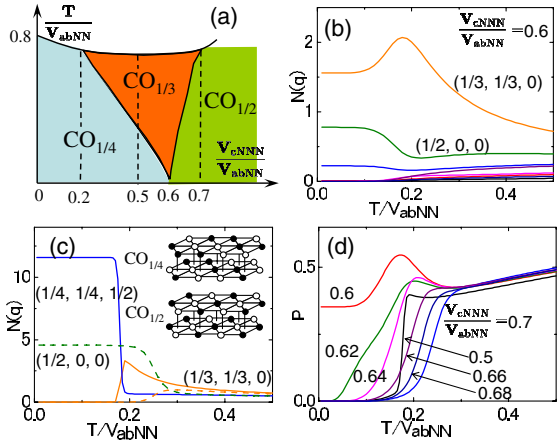

FIG. 2 (color online). (a) A mean-field phase diagram at finite T calculated in $\mathcal{H}_V$. (b) Charge correlation function $N(\mathbf{q})$ at $V_{cNNN}/V_{abNN} = 0.6$. (c) $N(\mathbf{q})$ at $V_{cNNN}/V_{abNN} = 0.5$ (bold lines) and 0.7 (broken lines). The insets show schematic views of the $CO_{1/4}$ and $CO_{1/2}$ structures. (d) Electric polarization P for several V_{cNNN}/V_{abNN} values. A value of V_{cNN}/V_{abNN} is chosen to be 1.2 in (a)–(d).

This sequential phase transition may explain the experiments in $YFe_2O_{4-\delta}$; the observed superlattice spots in the electron diffraction change from $(\frac{n}{3}\frac{n}{3}0)$ to $(\frac{n}{4}\frac{n}{4}0)$ with decreasing T [18]. The electric polarization is simulated by calculating $P = \langle p^2 \rangle^{1/2}$ [Fig. 2(d)]. We define $p = L^{-1}(\sum_{i\in U} - \sum_{i\in L})Q_i^z$, where $\sum_{i\in U(L)}$ represents a summation of sites in the upper (lower) layer. At $V_{\mathrm{cNNN}}/V_{\mathrm{abNN}} = 0.6$, a hump in P around $T/V_{\mathrm{abNN}} = 0.18$ corresponds to that in $N(\mathbf{q}_3)$ [19]. Apart from $V_{\mathrm{cNNN}}/V_{\mathrm{abNN}} = 0.6$, a reduction of P is correlated with the increases of $N(\mathbf{q}_2)$ and $N(\mathbf{q}_4)$.

The stability of the polar $CO_{1/3}$ is caused by the charge frustration and an entropy gain. Focus on the Fe sites located on the dotted lines in Fig. 1(b). The charge alignment at the Fe sites is responsible for the electric polarization. Since these sites are surrounded by three Fe^{2+} and three Fe^{3+} in the plane, the in-plane Coulomb interactions V_{abNN} are canceled out. Thus, the charge imbalance between the two layers occurs easily without loss of V_{abNN}, and the polar $CO_{1/3}$ is stabilized due to the interlayer Coulomb interactions. At these Fe sites, large charge fluctuation remains at finite T and contributes to an entropy gain. This situation in $CO_{1/3}$ is in contrast to $CO_{1/2}$ and $CO_{1/4}$, where all sites are equivalent.

Now we examine coupling between the electric polarization and the magnetic ordering. The Hamiltonian $\mathcal{H}_V + \mathcal{H}_J$ is analyzed in a pair of the $L \times L$ triangular lattices by utilizing the MUMC. The spin operators are set to be Ising spins, and the exchange constants are estimated by using the energy parameters for $LaFeO_3$ [20]. The orbital PS's in $\mathcal{H}_J$ are set to be zero, since the expected SO temperature is much higher than that for the orbital. The resulting P, $N(\mathbf{q})$ and the spin correlation functions $S(\mathbf{q})$ are plotted in Fig. 3. Around $T/V_{\mathrm{abNN}} = 0.18$ in Fig. 3(a), $N(\mathbf{q}_3)$ shows a shoulder, corresponding to a hump in $N(\mathbf{q}_3)$ calculated without $\mathcal{H}_J$. Further increase in $N(\mathbf{q}_3)$ occurs around the SO temperature $T/V_{\mathrm{abNN}} = 0.1$ [see Fig. 3(c)]. The temperature dependence of P [Fig. 3(b)] almost follows that of $N(\mathbf{q}_3)$. These results clearly show that the SO strongly stabilizes $CO_{1/3}$ accompanied by the electric polarization. The resulting SO is a ferrimagnetic structure characterized by the momentum $\mathbf{q}_3$ [Fig. 3(d)], which is consistent with the experiments [11,12].

The remarkable enhancement of the electric polarization below the SO temperature is caused by the spin-charge coupling and the spin frustration. Focus on the Fe^{2+} sites in the $2Fe^{3+}$-Fe^{2+} (upper) layer in Fig. 3(d). Since these Fe ions are surrounded by the NN three-up and three-down spins of Fe^{3+}, spin directions at the sites are not determined uniquely. There is a large number of degenerate spin states, which contribute to an entropy gain. Because this spin structure is realized on the polar $CO_{1/3}$, the electric polarization is reinforced through the spin-charge coupling in $\mathcal{H}_J$. In other words, a large entropy gain is induced by the charge imbalance in $CO_{1/3}$. Essence of this mechanism

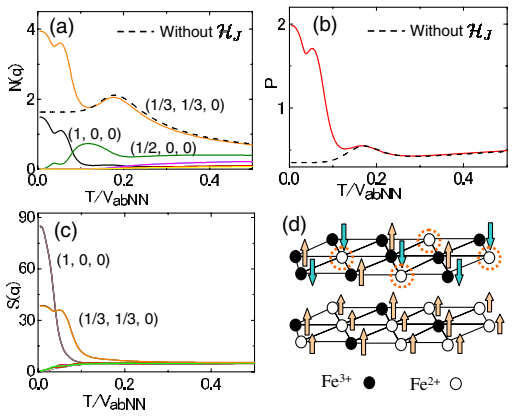

FIG. 3 (color online). Charge-correlation function $N(\mathbf{q})$ (a), electric polarization P (b), and spin correlation function $S(\mathbf{q})$ (c) calculated in $\mathcal{H}_V + \mathcal{H}_J$. A schematic view of the charge and spin structure below the ferrimagnetic ordering temperature is shown in (d). Spin directions at the sites marked by broken circles are not uniquely determined.

is based on the spin frustration due to the antiferromagnetic configuration for the Fe^{3+} spins, and does not depend on detailed parameter choice. The present study predicts the large ME response observed experimentally [10,13,14]. It is shown by the numerical calculation that by applying magnetic field in the CO/SO phase, the electric polarization is decreased considerably.

Finally, we pay our attention to the orbital state. Until now, there are no experimental reports for the long-range orbital order and/or the Jahn-Teller lattice distortion in RFe_2O_4. Thus, here we examine a possible orbital state in the CO/SO structure. By using the relation $\sum_l \pi_i^l = 0$, Hamiltonian $\mathcal{H}_J$ is mapped onto an effective orbital model defined on the Fe^{2+} honeycomb lattice in the $2Fe^{2+}$-Fe^{3+} (lower) layer [see Fig. 3(d)]. The model is derived as $\mathcal{H}_\tau = -J\sum_i(\tau_i^\alpha \tau_{i+\delta_\alpha}^\alpha + \tau_i^\beta \tau_{i+\delta_\beta}^\beta + \tau_i^\gamma \tau_{i+\delta_\gamma}^\gamma)$. Here, δ_l indicates a NN Fe-Fe bond labeled by directions $l = (\alpha, \beta, \gamma)$ [see Fig. 4(a)], and $J(>0)$ is the exchange constant. We redefine the orbital PS operator as $\tau_i^l = \cos(\pi/2 + 2\pi n_l/3)T_i^z + \sin(\pi/2 + 2\pi n_l/3)T_i^x$ with $(n_\alpha, n_\beta, n_\gamma) = (0, 1, 2)$. This operator represents a projection of $\mathbf{T_i}$ on the NN Fe-Fe bond direction. When (α, β, γ) is replaced by (x, y, z) in the Cartesian coordinate, this model corresponds to the e_g-orbital model [21,22]. A related model is examined in the quantum computation [23]. It is worth noting that the interaction between orbitals explicitly depends on the bond direction. Although the honeycomb lattice is bipartite, there are intrinsic frustration effects; when PS's are arranged to gain bond energy for one direction, these are not fully favorable for other bonds.

This model provides a nontrivial orbital state. The Hamiltonian is rewritten as $\mathcal{H}_\tau = (J/2)\sum_{\langle ij\rangle}(\tau_i^l - \tau_j^l)^2 - J\sum_{il}(\tau_i^l)^2$, where the second term becomes a numerical constant. This form indicates a large number of the classical degenerate GS which satisfy $\tau_i^l = \tau_j^l$ for each NN ij

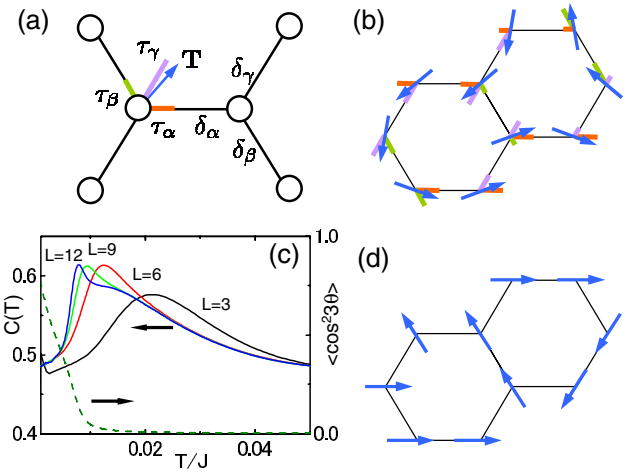

FIG. 4 (color online). (a) A schematic picture of the Fe^{2+} sublattice in the $2Fe^{2+}$-Fe^{3+} layer. Bold arrows and bold bars represent the orbital PS direction and the PS projection components τ_i^l on the NN bonds, respectively. (b) One of the ground state PS configurations. (c) Specific heat $C(T)$ for several cluster sizes. Broken line represents $\langle \cos^2 3\theta \rangle$ in $L = 12$. (d) One of the PS configurations at finite temperature below T_O.

pair. One of the PS configurations in the GS is shown in Fig. 4(b). The large degeneracy originates from the unusual orbital interaction. The momentum representation for the orbital interaction is given as $\mathcal{H}_\tau = \sum_{\mathbf{k}} \psi(\mathbf{k})^t \hat{J}(\mathbf{k}) \psi(\mathbf{k})$ with $\psi(\mathbf{k}) = [T_A^x(\mathbf{k}), T_A^z(\mathbf{k}), T_B^x(\mathbf{k}), T_B^z(\mathbf{k})]$ and a 4×4 matrix $\hat{J}(\mathbf{k})$. Here, A and B represent the two sublattices on the honeycomb lattice. The lowest eigenvalue for $\hat{J}(\mathbf{k})$ is a momentum-independent flat band at $-3J/4$. Thus, all eigenstates with different $\mathbf{k}$ provide the degenerate GS. At finite T, we analyze $\mathcal{H}_\tau$ on a $2 \times L \times L$ site cluster ($L = 3 \sim 12$) by using the MUMC, where the PS operators are treated as classical vectors in the T^x-T^z plane. In the specific heat $C(T)$ [Fig. 4(c)], a peak appears around $T/J = 0.025$ for $L = 3$. This temperature, denoted as T_O, is much lower than the mean-field ordering temperature $3J/8$. The peak shifts to lower T and becomes sharp with increasing L. We also calculate the orbital correlation functions $\mathcal{T}^{lm}(\mathbf{q}) = L^{-2} \sum_{ij} e^{i\mathbf{q}\cdot(\mathbf{r}_i - \mathbf{r}_j)} \langle T_i^l T_j^m \rangle$ ($l, m = x, z$) for all possible $\mathbf{q}$'s in clusters. However, the magnitudes are less than 20% of their maximum values, and remarkable increases in $\mathcal{T}^{lm}(\mathbf{q})$ are not observed with increasing L. We have found an order parameter, $\langle \cos^2 3\theta \rangle \equiv \langle [(2L^2)^{-1} \sum_i \cos 3\theta_i]^2 \rangle$, with the PS angle $\theta_i [\equiv \tan^{-1}(-T_i^z/T_i^x)]$. This parameter grows up below T_O and approaches to 1 [see Fig. 4(c)]. This result implies that θ_i at each site takes one of the three angles $(2\pi n)/3$ with $n = (0, 1, 2)$, or one of the three $(2\pi n + \pi)/3$. One configuration is shown in Fig. 4(d) where $(2L^2)^{-1} \sum_i \cos 3\theta_i = +1$. At $T = 0$, any values for θ_i are allowed, as long as the relation $\tau_i^l = \tau_j^l$ is satisfied. Values of θ_i are fixed to be $(2\pi n)/3$ or $(2\pi n + \pi)/3$ at finite T. This is the so-called order by fluctuation mechanism.

Summarizing, we present a theory of RFe_2O_4 as an exotic dielectric material with the CO driven electric polarization and the ME effects caused by the spin-charge coupling. The charge frustration allows the charge imbalance without inversion symmetry. This CO is reinforced by the magnetic ordering where the spin frustration contributes to the entropy gain. The present mechanism of the ME effects is different from the spin-lattice coupling mechanism proposed in the previous multiferroics, e.g., $RMnO_3$. A possible orbital state is examined in the CO/SO. A kind of the angle order of the orbital pseudospins grows up at low T. The present study provides an insight for searching of a new class of electronic multiferroics in correlated electron systems.

The authors would like to thank N. Ikeda, S. Mori, T. Arima, J. Akimitsu, M. Sasaki, M. Matsumoto, and H. Matsueda for their valuable discussions. This work was supported by JSPS KAKENHI (Nos. 16340094, 16104005) and TOKUTEI No. 451 (No. 18044001) from MEXT, NAREGI, and CREST.

*Present address: Japan Medical Materials Co., Osaka, 532-0003 Japan.

[1] T. Kimura *et al.*, Nature (London) **426**, 55 (2003).
[2] K. Saitoh *et al.*, J. Phys. Condens. Matter **7**, 2855 (1995).
[3] N. Hur *et al.*, Nature (London) **429**, 392 (2004).
[4] D. V. Efremov *et al.*, Nat. Mater. **3**, 853 (2004).
[5] Y. Tokunaga *et al.*, Nat. Mater. **5**, 937 (2006).
[6] P. Monceau *et al.*, Phys. Rev. Lett. **86**, 4080 (2001).
[7] S. Horiuchi *et al.*, Science **299**, 229 (2003).
[8] N. Kimizuka *et al.*, in *Handbook on the Physics and Chemistry of Rare Earth*, edited by K. A. Gshneider Jr. and L. Eyring (Elsevier, New York, 1990), Vol. 13, p. 283.
[9] Y. Yamada *et al.*, J. Phys. Soc. Jpn. **66**, 3733 (1997).
[10] N. Ikeda *et al.*, Nature (London) **436**, 1136 (2005).
[11] J. Akimitsu *et al.*, Solid State Commun. **32**, 1065 (1979).
[12] K. Shiratori *et al.*, *Proceedings of the 6th International Conference of Ferrites* (Japan Soc. Powder and Powder Metallurgy, Tokyo and Kyoto, 1992), p. 703.
[13] N. Ikeda *et al.*, Ferroelectrics **161**, 111 (1994).
[14] A. Subramanian *et al.*, Adv. Mater. **18**, 1737 (2006).
[15] The following discussion for orbital is also applicable to the case where the E'' orbitals are the lowest.
[16] A. Nagano *et al.*, J. Phys. Condens. Matter **19**, 145263 (2007).
[17] B. A. Berg, J. Stat. Phys. **82**, 323 (1996).
[18] N. Ikeda *et al.*, Ferroelectrics **286**, 175 (2003).
[19] With increasing the system size L at $V_{cNNN}/V_{abNN} = 0.6$, the hump in P around $T/V_{abNN} = 0.18$ grows up, and a value of P around $T = 0$ reduces. This is because $CO_{1/3}$ degenerates with a number of nonpolar CO with the momentum $\mathbf{q}_3$ at $T = 0$.
[20] T. Mizokawa and A. Fujimori, Phys. Rev. B **54**, 5368 (1996).
[21] T. Tanaka *et al.*, Phys. Rev. Lett. **95**, 267204 (2005).
[22] Z. Nussinov *et al.*, Europhys. Lett. **67**, 990 (2004).
[23] A. Y. Kitaev, Ann. Phys. (N.Y.) **321**, 2 (2006).